PAPER • OPEN ACCESS

Quasiclassical theory of the spin–orbit magnetoresistance of three-dimensional Rashba metals

View the article online for updates and enhancements.

IOP | ebooks™

Bringing you innovative digital publishing with leading voices to create your essential collection of books in STEM research.

Start exploring the collection - download the first chapter of every title for free.

New Journal of Physics

The open access journal at the forefront of physics

CrossMark

PAPER

Quasiclassical theory of the spin–orbit magnetoresistance of three-dimensional Rashba metals

Sebastian Tölle[1,3] ⓘ, Michael Dzierzawa[1], Ulrich Eckern[1] ⓘ and Cosimo Gorini[2]

1   Universität Augsburg, Institut für Physik, D-86135 Augsburg, Germany
2   Universität Regensburg, Institut für Theoretische Physik, 93040 Regensburg, Germany
3   Author to whom any correspondence should be addressed.

E-mail: sebastian.toelle@physik.uni-augsburg.de
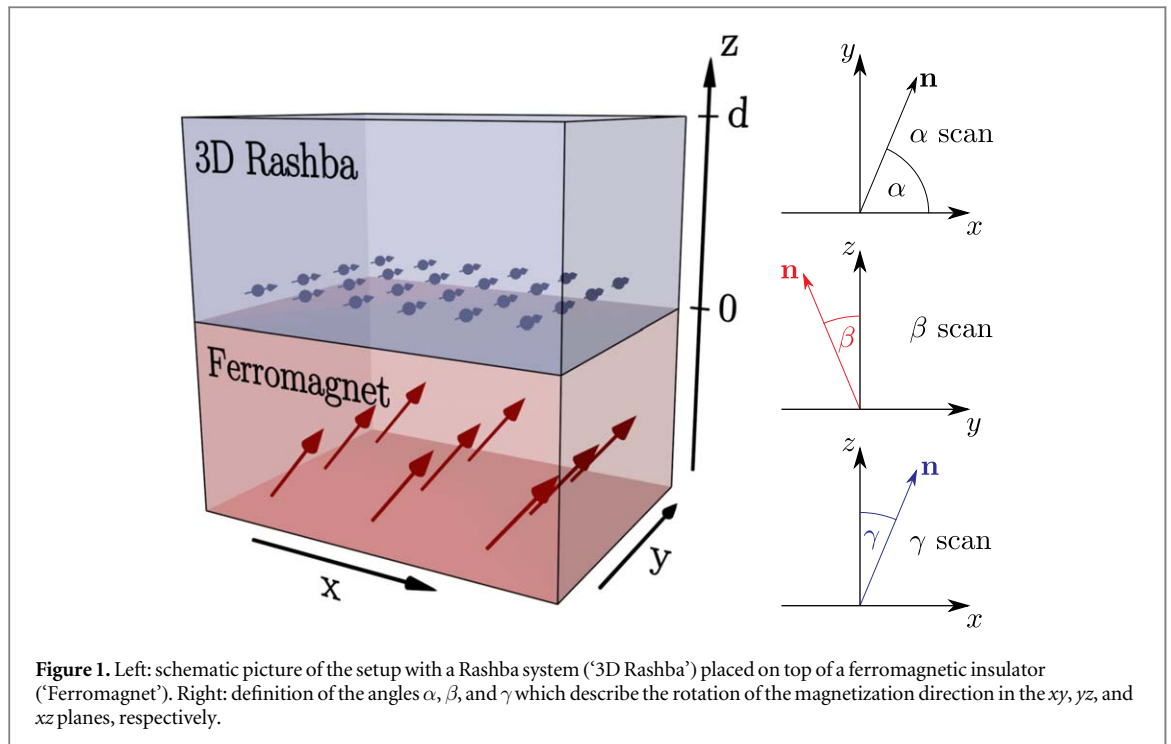
Abstract

The magnetoresistance of a three-dimensional Rashba metal placed on top of a ferromagnetic insulator is theoretically investigated. In addition to the intrinsic Rashba spin–orbit interaction, we consider extrinsic spin–orbit coupling via side-jump and skew scattering, as well as Elliott–Yafet spin relaxation. The latter is anisotropic due to the mass anisotropy which reflects the noncentrosymmetric crystal structure. A quasiclassical approach is employed to derive coupled spin-diffusion equations, which are supplemented by boundary conditions that account for the spin-transfer torque at the interface of the bilayer. The magnetoresistance is fully determined by the current-induced spin polarization, i.e., it cannot in general be ascribed to a single (bulk) spin Hall angle. Our theory reproduces several features of the experiments, at least qualitatively, and contains established phenomenological results in the relevant limiting cases. In particular, the anisotropy of the Elliott–Yafet spin relaxation mechanism plays a major role for the interpretation of the observed magnetoresistance.

1. Introduction

The fundamental tasks in the field of spintronics [1, 2] are to generate, manipulate, and detect spin densities or spin currents. One particularly interesting example where all these tasks are achieved simultaneously is the spin Hall magnetoresistance in a normal-metal/ferromagnet bilayer structure [3–5]. In this case, an electric current in the normal metal generates a spin current via the spin Hall effect [6–9]. This spin current gets only partly reflected at the interface to the adjacent ferromagnet, thereby exerting a torque on the magnetization [10–12]. The reflected spin current is converted back into a charge current due to the inverse spin Hall effect [13–15], resulting in a magnetization-dependent spin–orbit signature in the magnetoresistance.

Recently, a new type of spin–orbit-dependent magnetoresistance has gained considerable attention, the Rashba–Edelstein magnetoresistance [16, 17]. It relies on the inverse spin galvanic effect [18–20], a current-induced spin polarization due to spin–orbit coupling [21, 22], also known as Edelstein or Rashba–Edelstein effect [23] in systems with Rashba spin–orbit coupling [24, 25]. A typical experimental setup consists of a substrate/normal-metal/ferromagnet trilayer with a two-dimensional electron gas (2DEG) at the substrate/normal-metal interface. The magnetoresistance is usually explained as follows [16]: a current-induced spin polarization in the 2DEG leads to a spin current which flows through the normal metal, gets reflected at the normal-metal/ferromagnet interface, and is then converted back again to a charge current in the 2DEG via the spin galvanic effect [26, 27].

However, in dirty Rashba systems the interplay between extrinsic effects (due to impurities) and intrinsic effects (due to the band or device structure) leads to a non-trivial interaction of spin densities and spin currents [2, 28]. Accordingly, the various spin–orbit signatures, e.g. via the spin galvanic and the (in-plane) inverse spin Hall effect, in charge signals are hard to separate [29, 30], eventually leading to a non-trivial magnetization dependence of the magnetoresistance [31]. Additional contributions such as the anisotropic magnetoresistance

Figure 1. Left: schematic picture of the setup with a Rashba system ('3D Rashba') placed on top of a ferromagnetic insulator ('Ferromagnet'). Right: definition of the angles α, β, and γ which describe the rotation of the magnetization direction in the *xy*, *yz*, and *xz* planes, respectively.

in ferromagnetic metals, or spin Hall effects and/or a field-dependent magnetoresistance in the substrate/ normal-metal part of the trilayer structure [17], complicate the separation of Rashba-related effects from confounding signals[4].

One possibility to overcome these problems is to consider a bilayer consisting of a three-dimensional (3D) system with Rashba spin–orbit coupling and an insulating ferromagnet. Although commonly associated with (quasi) two-dimensional asymmetric systems, there exists a new class of bulk 3D Rashba metals [33–35] with rather strong Rashba spin–orbit coupling due to their noncentrosymmetric crystal structure. Obviously, these materials offer an interesting playground for investigations of Rashba-associated signatures in the charge sector, e.g., the anisotropy of the dc conductivity [36]. Notice also that recent experiments in Pt thin films on MgO and GaAs substrates show evidence of Rashba-like spin–orbit coupling [37]. Analogously, thin films with built-in asymmetry, such as the Pt-decorated Cu[Pt]/YIG setup studied in [38], can be considered as effective Rashba metals.

In this article, we theoretically investigate the magnetoresistance of 3D Rashba metals, taking into account a mass anisotropy and both Dyakonov–Perel and Elliott–Yafet spin relaxation. To be consistent, we additionally consider extrinsic spin–orbit coupling via side-jump and skew scattering, hence our theory goes substantially beyond phenomenological approaches to the spin Hall magnetoresistance in heavy-metal/ferromagnet bilayers [39], but recovers their results in the appropriate limiting cases. Essentially, we show that in composite systems made of a ferromagnet and an anisotropic metal where Rashba and extrinsic spin–orbit coupling coexist, magnetoresistance signals are determined by current-induced spin polarizations. In other words, such signals do not allow access to a single, well-defined (bulk) spin Hall angle, unless specific limiting conditions are met.

Our paper is organized as follows. We specify the boundary conditions and introduce the model of the system under consideration in section 2. Section 3 focuses on the current-induced spin polarization, paving the way for a consistent description of the magnetoresistance as presented in section 4. We briefly conclude in section 5.

2. The model

The setup under consideration is schematically depicted in figure 1. It consists of a 3D Rashba metal of thickness d which is placed on top of a ferromagnetic insulator with the interface at $z = 0$. The ferromagnet offers the possibility to manipulate the spin current across the interface due to the spin transfer torque by varying the magnetization direction **n**. In this work, the boundary condition for the spin current in the Rashba metal at the

---

[4] In narrow gap semiconductors with strong Zeeman splitting the magnetoresistance can also be affected by Rashba field fluctuations, see [32].

interface is taken as [40, 41]

$$\mathbf{j}_z(0) = \frac{1}{2\pi\hbar N_0}[g_r^{\uparrow\downarrow}\mathbf{n}\times(\mathbf{n}\times\mathbf{s}(0)) + g_i^{\uparrow\downarrow}\mathbf{n}\times\mathbf{s}(0)], \tag{1}$$

where $g_r^{\uparrow\downarrow}$ and $g_i^{\uparrow\downarrow}$ are the real and the imaginary part of the spin mixing conductance[5]. Here, $N_0 = m_\parallel\sqrt{2m_\perp\epsilon_F}/2\pi^2\hbar^3$ is the density of states per spin and volume at the Fermi energy of the 3D Rashba metal, which is described by the model Hamiltonian

$$H = \frac{p_x^2 + p_y^2}{2m_\parallel} + \frac{p_z^2}{2m_\perp} - \frac{\alpha_R}{\hbar}(\mathbf{p}\times\boldsymbol{\sigma})\cdot\mathbf{e}_z + H_{\mathrm{imp}}, \tag{2}$$

where α_R is the Rashba coefficient, and $\boldsymbol{\sigma} = (\sigma^x, \sigma^y, \sigma^z)$ is the vector of Pauli matrices. The inversion symmetry breaking direction $\mathbf{e}_z$ accounts for the noncentrosymmetric crystal structure. Correspondingly, $m_\parallel$ and $m_\perp$ are the in-plane and out-of-plane effective masses. We emphasize that the Hamiltonian (2) can actually be taken as a model for a rather large number of systems. For example: (i) inversion-asymmetric metal/(insulating)substrate bilayers, as long as the thickness d of the metallic layer does not substantially exceed the electronic phase-coherence length. Such a condition, which in particular justifies an anisotropic effective mass, is easily met in low-temperature experiments [37]; (ii) intrinsically anisotropic 'decorated' bilayers, such as the Cu[Pt]/YIG setup studied in [38], where Cu is sputtered with Pt nanoislands.

Disorder due to nonmagnetic impurities is taken into account by

$$H_{\mathrm{imp}} = V + \frac{\lambda^2}{4\hbar}\boldsymbol{\sigma}\cdot(\nabla V\times\mathbf{p}), \tag{3}$$

where λ is the effective Compton wavelength, and V is a δ-correlated random potential.

Based on this microscopic model, we use a generalized Boltzmann equation for the distribution function $f = f^0 + \mathbf{f}\cdot\boldsymbol{\sigma}$ as derived in [44]. Here, f^0 and $\mathbf{f}$ are the charge and the spin distribution functions which yield the spin density

$$\mathbf{s} = \int\frac{\mathrm{d}^3p}{(2\pi\hbar)^3}\mathbf{f}, \tag{4}$$

and the charge and spin current in $i = x, y, z$ direction,

$$j_i = -2e\int\frac{\mathrm{d}^3p}{(2\pi\hbar)^3}v_i f^0, \tag{5}$$

$$\mathbf{j}_i = \int\frac{\mathrm{d}^3p}{(2\pi\hbar)^3}v_i\mathbf{f}, \tag{6}$$

where v_i is the ith component of the velocity $\mathbf{v} = (p_x/m_\parallel, p_y/m_\parallel, p_z/m_\perp)$. For technical details regarding the Boltzmann equation and the derivation of the transport equations used in the following sections we refer to appendix A. Similar equations were also considered elsewhere [45–48], albeit in a form not well suited to our purposes—notably because of the complicated structure of the velocity operator and the collision integral.

Disorder, as taken into account by H_{imp}, leads to momentum relaxation, $1/\tau$, and two types of spin relaxation: Dyakonov–Perel relaxation due to Rashba spin–orbit coupling, and Elliott–Yafet relaxation due to spin–orbit interaction with the random potential. Both relaxation mechanisms are anisotropic,

$$\partial_t\mathbf{s} \sim -\frac{1}{\tau_{\mathrm{DP}}}\begin{pmatrix}1 & 0 & 0\\ 0 & 1 & 0\\ 0 & 0 & 2\end{pmatrix}\mathbf{s} - \frac{1}{\tau_s}\begin{pmatrix}1 & 0 & 0\\ 0 & 1 & 0\\ 0 & 0 & \zeta\end{pmatrix}\mathbf{s}, \tag{7}$$

where $1/\tau_{\mathrm{DP}}$ and $1/\tau_s$ are the Dyakonov–Perel and Elliott–Yafet relaxation rates, respectively. In the dirty regime, the former is given by

$$\frac{1}{\tau_{\mathrm{DP}}} = \left(\frac{2m_\parallel\alpha_R}{\hbar^2}\right)^2 D_\parallel \tag{8}$$

with the in-plane diffusion constant $D_\parallel = 2\epsilon_F\tau/3m_\parallel$. The anisotropy of the Elliott–Yafet mechanism depends on the masses via the parameter

---

[5] More generally, the spin mixing conductance $g^{\uparrow\downarrow}$ is a 3 × 3 matrix [42]. However, we assume $\alpha_R/\hbar v_F \ll 1$, in accordance with the condition discussed in the beginning of section 3; in this limit, the spin mixing conductance is proportional to a unit matrix. In the present work, we consider $g^{\uparrow\downarrow}$ as a parameter. References [42, 43] discuss some aspects of the microscopic derivation of these parameters for interfaces with spin–orbit coupling.

$$\zeta = \frac{2m_\perp}{m_\perp + m_\parallel}, \tag{9}$$

and the corresponding relaxation rate is given by[6]

$$\frac{1}{\tau_s} = \frac{8}{9(2-\zeta)}\left(\frac{\lambda p_F}{2\hbar}\right)^4 \frac{1}{\tau}, \tag{10}$$

with $p_F = \sqrt{2m_\parallel \epsilon_F}$. Note that $\tau_{\mathrm{DP}}/\tau_s \sim \tau^{-2}$ can be enhanced by increasing the temperature, since τ^{-1} is typically an increasing function of the temperature in a metallic system.

3. Current-induced spin polarization

In this section, we investigate the current-induced spin polarization in the spin diffusive limit, in the sense that $p_F \tau/m_\parallel l_{\mathrm{DP}} \ll 1$, where $l_{\mathrm{DP}} = \sqrt{D_\parallel \tau_{\mathrm{DP}}} = \hbar^2/(2m_\parallel \alpha_R)$. Neglecting spin-dependent contributions to the charge current (thus $j_x \approx \sigma_{\mathrm{D}} E_x$, where σ_{D} is the Drude conductivity) the Boltzmann equation yields the following set of diffusion equations for the spin density:

$$q_1^2 s^x = \nabla_z^2 s^x, \tag{11}$$

$$q_1^2 s^y = \nabla_z^2 s^y + q_1^2 s_0^y, \tag{12}$$

$$q_2^2 s^z = \nabla_z^2 s^z. \tag{13}$$

The inverse spin relaxation lengths q_1 and q_2 are given by

$$q_1 = \frac{1}{l_{\mathrm{DP}}}\sqrt{\frac{m_\perp}{m_\parallel}\left(1 + \frac{\tau_{\mathrm{DP}}}{\tau_s}\right)}, \tag{14}$$

$$q_2 = \frac{1}{l_{\mathrm{DP}}}\sqrt{\frac{m_\perp}{m_\parallel}\left(2 + \zeta\frac{\tau_{\mathrm{DP}}}{\tau_s}\right)}. \tag{15}$$

We have also introduced the bulk current-induced spin polarization in the homogeneous case,

$$s_0^y = -\frac{1}{D_\parallel q_{\mathrm{isg}}}\frac{\sigma_{\mathrm{D}} E_x}{2e}, \tag{16}$$

where q_{isg} ('isg' = inverse spin galvanic) is defined by

$$\frac{1}{D_\parallel q_{\mathrm{isg}}} = \frac{\tau_s/l_{\mathrm{DP}}}{1 + \tau_s/\tau_{\mathrm{DP}}}(\xi_{\mathrm{int}}\theta_{\mathrm{int}}^{\mathrm{sH}} + \theta_{\mathrm{ext}}^{\mathrm{sH}}). \tag{17}$$

Here, $\theta_{\mathrm{int}}^{\mathrm{sH}} = \alpha_R \tau/\hbar l_{\mathrm{DP}}$ accounts for the Rashba contribution to the spin Hall angle[7], and

$$\xi_{\mathrm{int}} = 1 - \frac{\tau_{\mathrm{DP}}}{\tau_s}\left(1 - \frac{3\zeta}{4}\right). \tag{18}$$

Equation (16) describes the inverse spin galvanic effect in an anisotropic Rashba metal, explicitly taking into account side-jump and skew scattering via the parameter $\theta_{\mathrm{ext}}^{\mathrm{sH}}$, the extrinsic contribution to the spin Hall angle[8].

To proceed, we explicitly solve equations (11)–(13) by fixing the boundary conditions at $z = 0$ and $z = d$. These are given by equation (1) and the condition $\mathbf{j}_z(d) = 0$, corresponding to spin-conserving scattering[9]. We obtain

$$s^y(z) = s_0^y + \Delta s_{\mathrm{sc}}^y(z) + \Delta s^y(z, \mathbf{n}), \tag{19}$$

where

$$\Delta s_{\mathrm{sc}}^y(z) = \frac{\theta_{\mathrm{ext}}^{\mathrm{sH}}}{D_\parallel q_1}\frac{\sigma_{\mathrm{D}} E_x}{2e}\frac{\sinh(q_1(d/2 - z))}{\cosh(q_1 d/2)} \tag{20}$$

is the spin accumulation which arises due to the spin current j_z^y even in the absence of the ferromagnet. The magnetization-dependent contribution is given by $\Delta s^y(z, \mathbf{n})$. In the following, we focus on $\Delta s^y(z, \mathbf{n})$ with the magnetization vector lying in the xy, yz, or xz plane, respectively, i.e., the α, β, and γ scans as defined in figure 1.

---

[6] A brief outline of the Elliott–Yafet spin relaxation as described within the Boltzmann theory is given in appendix A.

[7] Note that $\theta_{\mathrm{int}}^{\mathrm{sH}}$ is not the bulk spin Hall angle in case of a pure Rashba system, see [28].

[8] More precisely, $\theta_{\mathrm{ext}}^{\mathrm{sH}} = \theta_{\mathrm{sj}}^{\mathrm{sH}} + \theta_{\mathrm{ss}}^{\mathrm{sH}}$, where $\theta_{\mathrm{sj,ss}}^{\mathrm{sH}} = 2e\sigma_{\mathrm{sj,ss}}^{\mathrm{sH}}/\sigma_{\mathrm{D}}$ with the side-jump and skew scattering contributions to the spin Hall conductivity, $\sigma_{\mathrm{sj}}^{\mathrm{sH}}$ and $\sigma_{\mathrm{ss}}^{\mathrm{sH}}$, being defined in [28], respectively.

[9] For a more detailed discussion of boundary conditions for two-dimensional Rashba or Dresselhaus systems, see, e.g., [47, 49–51].

After some algebra, we obtain

$$\Delta s^y_{\alpha,\beta,\gamma}(z) = -A(z)f_{\alpha,\beta,\gamma},\tag{21}$$

with

$$A(z) = s^y_0\left[1 - \tanh\left(\frac{q_1 d}{2}\right)\theta^{\mathrm{sH}}_{\mathrm{ext}}\frac{q_{\mathrm{isg}}}{q_1}\right]\frac{\cosh(q_1(d-z))}{\cosh(q_1 d)}.\tag{22}$$

The angular dependence is given by

$$f_\alpha = \frac{(q_i^2 + q_r^2 + q_r\tilde{q}_2)\cos^2\alpha}{q_i^2 + (\tilde{q}_1 + q_r)(\tilde{q}_2 + q_r)},\tag{23}$$

$$f_\beta = \frac{(q_i^2 + q_r^2 + q_r\tilde{q}_1)\cos^2\beta}{\frac{\tilde{q}_1}{\tilde{q}_2}[q_i^2 + (\tilde{q}_1 + q_r)(\tilde{q}_2 + q_r)]\sin^2\beta + [q_i^2 + (\tilde{q}_1 + q_r)^2]\cos^2\beta},\tag{24}$$

$$f_\gamma = \frac{q_i^2 + q_r^2 + q_r\tilde{q}_1 - (q_i^2 + q_r^2)\left(1 - \frac{\tilde{q}_1}{\tilde{q}_2}\right)\sin^2\gamma}{\frac{\tilde{q}_1}{\tilde{q}_2}[q_i^2 + (\tilde{q}_1 + q_r)(\tilde{q}_2 + q_r)]\sin^2\gamma + [q_i^2 + (\tilde{q}_1 + q_r)^2]\cos^2\gamma},\tag{25}$$

where the respective scan is indicated by the subscript. Furthermore, we have introduced $q_{r,i} = g^{\uparrow\downarrow}_{r,i}/2\pi\hbar N_0 D_\perp$, where $D_\perp = 2\epsilon_F\tau/3m_\perp$ is the out-of-plane diffusion constant, and $\tilde{q}_{1,2} = q_{1,2}\tanh(q_{1,2}d)$. An outline of the derivation is given in appendix B. Equations (21)–(25) explicitly describe how the spatially resolved spin polarization in an anisotropic Rashba metal depends on the magnetization direction of the adjacent ferromagnet. We wish to point out that these equations fully determine the magnetoresistance signals, as we shall see in the following section.

4. Magnetoresistance

The resistivity ρ is defined by

$$E_x = \rho j_x,\tag{26}$$

where E_x is the electric field, and $j_x = d^{-1}\int_0^d \mathrm{d}z\, j_x(z)$ is the current density averaged over the thickness of the Rashba system. In the following, quantities without explicit z dependence are considered as thickness-averaged. Regarding the magnetoresistance, it is convenient to split the resistivity,

$$\rho = \rho_0 + \Delta\rho(\mathbf{n}),\tag{27}$$

where $\rho_0 \approx 1/\sigma_{\mathrm{D}}$ is the resistivity for vanishing spin-mixing conductance, $g^{\uparrow\downarrow}_r = g^{\uparrow\downarrow}_i = 0$, and $\Delta\rho$ captures the magnetization dependence. From the generalized Boltzmann equation, see appendix A, one obtains

$$j_x(z) = \sigma_{\mathrm{D}}E_x + 2e\left[\frac{l_{\mathrm{DP}}}{\tau_s}\left(1 - \frac{3\zeta}{4}\right)\theta^{\mathrm{sH}}_{\mathrm{int}}s^y(z) - (\theta^{\mathrm{sH}}_{\mathrm{int}} + \theta^{\mathrm{sH}}_{\mathrm{ext}})j^z_y(z) + \frac{m_\perp}{m_\parallel}\theta^{\mathrm{sH}}_{\mathrm{ext}}j^y_z(z)\right].\tag{28}$$

Loosely speaking, the first term in the square brackets corresponds to the spin galvanic or inverse Edelstein effect, the second term to the in-plane inverse spin Hall effect, and the third term to the out-of-plane inverse spin Hall effect. Interestingly, the relevant spin currents,

$$j^z_y(z) = \frac{l_{\mathrm{DP}}}{\tau_{\mathrm{DP}}}s^y(z) + (\theta^{\mathrm{sH}}_{\mathrm{int}} + \theta^{\mathrm{sH}}_{\mathrm{ext}})\frac{\sigma_{\mathrm{D}}E_x}{2e},\tag{29}$$

$$j^y_z(z) = -D_\perp\nabla_z s^y(z) - \theta^{\mathrm{sH}}_{\mathrm{ext}}\frac{m_\parallel}{m_\perp}\frac{\sigma_{\mathrm{D}}E_x}{2e},\tag{30}$$

are completely determined by $\Delta s^y(z,\mathbf{n})$ regarding their dependence on the magnetization of the ferromagnet. Hence, the angular dependence of $j_x(z)$, and thus the magnetoresistance, can be traced back to $\Delta s^y(z,\mathbf{n})$.

With the definition of the conductivity, $j_x = \sigma E_x$, where $\sigma = \sigma_0 + \Delta\sigma(\mathbf{n})$, analogously to equation (27), we obtain

$$\Delta\sigma(\mathbf{n})E_x = -2eD_\parallel q_{\mathrm{sg}}\Delta s^y(\mathbf{n}).\tag{31}$$

Here, we have introduced

$$q_{\mathrm{sg}} = \frac{1}{l_{\mathrm{DP}}}[\xi_{\mathrm{int}}\theta^{\mathrm{sH}}_{\mathrm{int}} + \xi_{\mathrm{ext}}\theta^{\mathrm{sH}}_{\mathrm{ext}}],\tag{32}$$

a wave number which represents the efficiency of the spin galvanic effect, with

$$\xi_{\text{ext}} = 1 - q_1 l_{\text{DP}} \tanh(q_1 d/2), \tag{33}$$

and ξ_{int} as defined in equation (18). For a thin system, $q_1 d \ll 1$, and assuming $q_1 l_{\text{DP}} \lesssim 1$, the second term on the rhs of equation (33) is negligible. Equivalently, the last term in the square brackets of equation (28), after averaging wrt the thickness, is small, which means that the out-of-plane spin current j_z^y does not contribute to the magnetoresistance, similar to a strictly 2D system.

Assuming $\sigma_0 \approx \sigma_D \gg \Delta\sigma$, the magnetization-dependent part of the resistivity is given by

$$\frac{\Delta\rho(\mathbf{n})}{\rho_0} \approx -\frac{\Delta\sigma(\mathbf{n})}{\sigma_D}. \tag{34}$$

We insert equation (31) together with the thickness average of $\Delta s_{\alpha,\beta,\gamma}^y(z)$, equation (21), and obtain the magnetoresistance ratio

$$\frac{\Delta\rho_{\alpha,\beta,\gamma}}{\rho_0} = C f_{\alpha,\beta,\gamma} \tag{35}$$

for the α, β, and γ scans, respectively. The magnitude of the effect is determined by

$$C = \frac{\tanh(q_1 d)}{q_1 d} \frac{q_{\text{sg}}}{q_{\text{isg}}} \left[1 - \tanh\left(\frac{q_1 d}{2}\right) \theta_{\text{ext}}^{\text{sH}} \frac{q_{\text{isg}}}{q_1} \right], \tag{36}$$

with the ratio $q_{\text{sg}}/q_{\text{isg}}$ being quadratic in the spin Hall angles. However, due to the simultaneous contributions from s^y, j_y^z, and j_z^y, the magnetoresistance *cannot* generally be expressed in terms of the square of a single total spin Hall angle θ_{sH}, as in the phenomenological approach [39]. Only in the special case where intrinsic spin–orbit coupling is negligible, the magnetoresistance can be expressed in terms of a single spin Hall angle squared. In the following, we discuss the magnetoresistance for the representative limits of a purely damping-like torque, $g_i^{\uparrow\downarrow} = 0$, and a purely field-like torque, $g_r^{\uparrow\downarrow} = 0$, respectively.

4.1. Damping-like torque
In the case of a vanishing imaginary part of the spin mixing conductance, $g_i^{\uparrow\downarrow} = 0$, which corresponds to a damping-like torque, the angular-dependent magnetoresistances are given by

$$\frac{\Delta\rho_\alpha}{\rho_0} = \frac{C q_r}{q_r + \tilde{q}_1} \cos^2\alpha, \tag{37}$$

$$\frac{\Delta\rho_\beta}{\rho_0} = \frac{C q_r \cos^2\beta}{q_r + \tilde{q}_1 - q_r\left(1 - \frac{\tilde{q}_1}{\tilde{q}_2}\right)\sin^2\beta}, \tag{38}$$

$$\frac{\Delta\rho_\gamma}{\rho_0} = \frac{C q_r}{q_r + \tilde{q}_1}. \tag{39}$$

We see that $\Delta\rho_\gamma$ is constant, and that $\Delta\rho_\beta$ has a similar angular dependence as $\Delta\rho_\alpha$ for a wide range of parameters. More precisely, in the case $|1 - \tilde{q}_1/\tilde{q}_2| \ll 1$, the $\sin^2\beta$ term in the denominator in equation (38) leads to higher harmonics in β of smaller magnitude,

$$\frac{\Delta\rho_\beta}{\rho_0} \approx \frac{C q_r}{q_r + \tilde{q}_1} \left[\cos^2\beta + \frac{1 - \tilde{q}_1/\tilde{q}_2}{4(1 + \tilde{q}_1/q_r)} \sin^2(2\beta) \right]. \tag{40}$$

Apparently, the ratio $\tilde{q}_1/\tilde{q}_2$ determines the sign of the next-to-leading harmonic of the signal.

Figure 2 shows the magnetoresistance according to equations (37)–(39). Panel (a) corresponds to the case where Rashba spin–orbit coupling is large compared to the extrinsic spin–orbit coupling, whereas (b) corresponds to the opposite limit. When Rashba spin–orbit coupling dominates the signal is larger by roughly an order of magnitude as compared to the extrinsic-dominated case. However, the angular dependence is very similar in the two regimes.

4.2. Field-like torque
In order to elucidate the effect of a purely field-like torque, we now neglect the real part of the spin mixing conductance, $g_r^{\uparrow\downarrow} = 0$. The angular-dependent magnetoresistances are then given by

$$\frac{\Delta\rho_\alpha}{\rho_0} = \frac{C q_i^2}{q_i^2 + \tilde{q}_1 \tilde{q}_2} \cos^2\alpha, \tag{41}$$
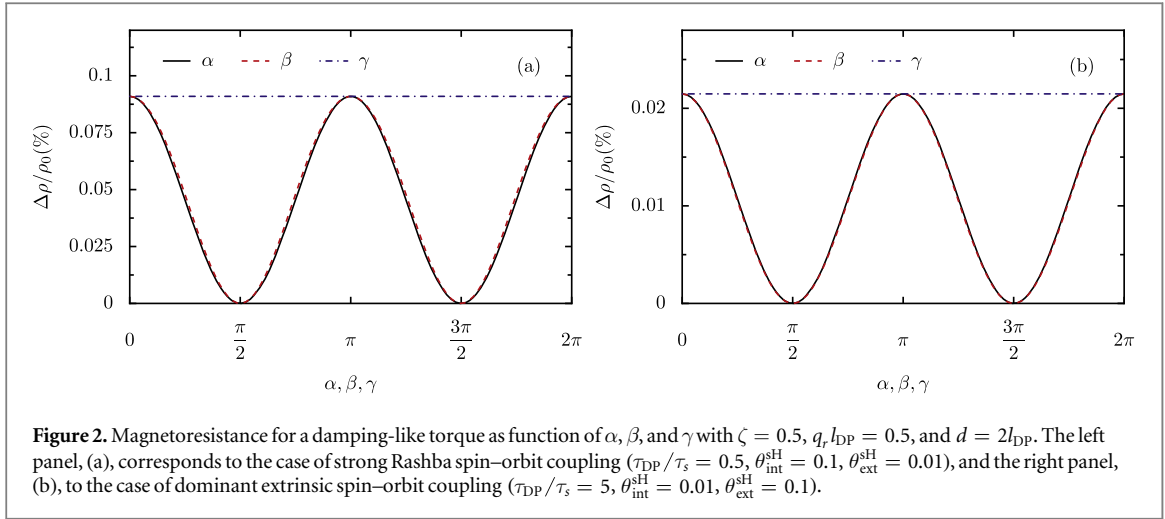
Figure 2. Magnetoresistance for a damping-like torque as function of α, β, and γ with $\zeta = 0.5$, $q_r l_{DP} = 0.5$, and $d = 2l_{DP}$. The left panel, (a), corresponds to the case of strong Rashba spin–orbit coupling ($\tau_{DP}/\tau_s = 0.5$, $\theta_{int}^{sH} = 0.1$, $\theta_{ext}^{sH} = 0.01$), and the right panel, (b), to the case of dominant extrinsic spin–orbit coupling ($\tau_{DP}/\tau_s = 5$, $\theta_{int}^{sH} = 0.01$, $\theta_{ext}^{sH} = 0.1$).

$$\frac{\Delta\rho_\beta}{\rho_0} = \frac{Cq_i^2\cos^2\beta}{q_i^2 + \tilde{q}_1^2 - q_i^2\left(1 - \frac{\tilde{q}_1}{\tilde{q}_2}\right)\sin^2\beta}, \tag{42}$$

$$\frac{\Delta\rho_\gamma}{\rho_0} = \frac{Cq_i^2\left[1 - \left(1 - \frac{\tilde{q}_1}{\tilde{q}_2}\right)\sin^2\gamma\right]}{q_i^2 + \tilde{q}_1^2 - q_i^2\left(1 - \frac{\tilde{q}_1}{\tilde{q}_2}\right)\sin^2\gamma}. \tag{43}$$

The ratio $\tilde{q}_1/\tilde{q}_2$ defines the sign of the $\sin^2\gamma$ contribution in equation (43). It also determines whether the ratio of the amplitudes of $\Delta\rho_\alpha$ and $\Delta\rho_\beta$,

$$\frac{\Delta\rho_\alpha(0)}{\Delta\rho_\beta(0)} = 1 - \frac{\tilde{q}_1\tilde{q}_2}{q_i^2 + \tilde{q}_1\tilde{q}_2}\left(1 - \frac{\tilde{q}_1}{\tilde{q}_2}\right), \tag{44}$$

is larger or smaller than one. For $\tilde{q}_1\tilde{q}_2 \gg q_i^2$ equation (44) reduces to

$$\frac{\Delta\rho_\alpha(0)}{\Delta\rho_\beta(0)} \approx \frac{\tilde{q}_1}{\tilde{q}_2}, \tag{45}$$

such that the ratio $\tilde{q}_1/\tilde{q}_2$ can be read off directly from the measured amplitudes of the α and β signals. Inserting the definitions of $\tilde{q}_1$ and $\tilde{q}_2$, equations (14) and (15), into equation (45), we can solve for

$$\frac{\tau_{DP}}{\tau_s} = \frac{2\left(\frac{\Delta\rho_\alpha(0)}{\Delta\rho_\beta(0)}\right)^2 - 1}{1 - \zeta\left(\frac{\Delta\rho_\alpha(0)}{\Delta\rho_\beta(0)}\right)^2}, \tag{46}$$

or, in case $\tau_{DP} \gg \tau_s$, directly extract the anisotropy parameter of the Elliott–Yafet spin relaxation,

$$\zeta \approx \left(\frac{\Delta\rho_\alpha(0)}{\Delta\rho_\beta(0)}\right)^{-2}. \tag{47}$$

Analogous to the damping-like case, up to linear order in $(1 - \tilde{q}_1/\tilde{q}_2)$, we can expand $\Delta\rho_\beta$ in terms of harmonics in β,
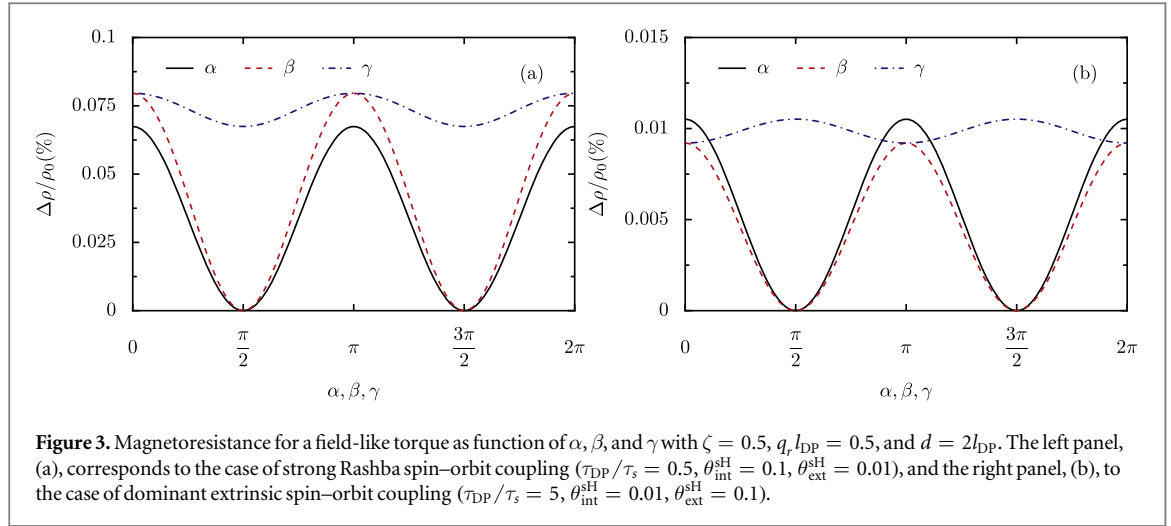
$$\frac{\Delta\rho_\beta}{\rho_0} \approx \frac{Cq_i^2}{q_i^2 + \tilde{q}_1^2}\left[\cos^2\beta + \frac{1}{4}\left(\frac{1 - \tilde{q}_1/\tilde{q}_2}{1 + \tilde{q}_1^2/q_i^2}\right)\sin^2(2\beta)\right], \tag{48}$$

and similarly $\Delta\rho_\gamma$ can be expressed as

$$\frac{\Delta\rho_\gamma}{\rho_0} \approx \frac{Cq_i^2}{q_i^2 + \tilde{q}_1^2}\left[1 - \frac{\tilde{q}_1^2}{q_i^2}\left(\frac{1 - \tilde{q}_1/\tilde{q}_2}{1 + \tilde{q}_1^2/q_i^2}\right)\sin^2\gamma\right]. \tag{49}$$

We see that one can obtain the ratio $q_i/\tilde{q}_1$ by dividing the amplitude of the second-harmonic of $\Delta\rho_\beta$ by the amplitude of the γ scan of the magnetoresistance.

Figure 3. Magnetoresistance for a field-like torque as function of α, β, and γ with $\zeta = 0.5$, $q_r l_{DP} = 0.5$, and $d = 2l_{DP}$. The left panel, (a), corresponds to the case of strong Rashba spin–orbit coupling ($\tau_{DP}/\tau_s = 0.5$, $\theta_{int}^{sH} = 0.1$, $\theta_{ext}^{sH} = 0.01$), and the right panel, (b), to the case of dominant extrinsic spin–orbit coupling ($\tau_{DP}/\tau_s = 5$, $\theta_{int}^{sH} = 0.01$, $\theta_{ext}^{sH} = 0.1$).

4.3. Discussion

First, we emphasize that our work allows a microscopic description of the magnetoresistance in anisotropic Rashba systems. The theory is not only applicable to real Rashba metals, but also to heavy-metal/ferromagnet bilayers, and substantially extends established phenomenological approaches [39]. The latter are contained in our results by setting $\zeta = 1$, $\alpha_R = 0$, and $\theta_{ext}^{sH} \to \theta_{sH}$.

Second, we wish to stress the following two aspects: (1) the consideration of a mass anisotropy, and (2) the inclusion of Rashba spin–orbit coupling. The mass anisotropy, point (1), leads to an anisotropic spin relaxation, even in the case of vanishing Rashba spin–orbit coupling $\alpha_R = 0$, and thus $\tilde{q}_1/\tilde{q}_2 \neq 1$. In this case, according to equation (25) the γ scan acquires a finite amplitude $\Delta\rho_\gamma$ when the imaginary part of the spin mixing conductance is nonzero, $g_i^{\uparrow\downarrow} \neq 0$. Hence, using a ferromagnetic insulator, one can extract the ratio of the reduced spin relaxation lengths $1/\tilde{q}_1$ and $1/\tilde{q}_2$ by a precise measurement of $\Delta\rho_\gamma$. Indeed, experimental results for a Cu[Pt]/YIG bilayer structure, where the Cu/YIG interface is sputtered with Pt nanosize islands, show a noticeable oscillation in the γ scan [38], which can be explained within our theory assuming a nonzero $g_i^{\uparrow\downarrow}$ and $\tilde{q}_1/\tilde{q}_2 > 1$, cf figure 3(b). This effect is quite pronounced due to an enhancement of the anisotropy of the spin relaxation mechanism as the sputtered Pt exhibits Rashba spin–orbit coupling [38]. A pronounced oscillation in the γ scan was also observed in a very recent experiment employing a Pt ultra-thin film deposited on the ferromagnetic insulator $LaCoO_3$ [43].

This directly brings us to point (2). There is evidence that thin Pt films also possess a strong Rashba spin–orbit coupling [37]. In this case, the inverse spin galvanic effect strongly influences the spin transport, and the magnetoresistance signal cannot be interpreted as spin Hall magnetoresistance in the sense of a 'simple' interplay between the spin Hall and the inverse spin Hall effect, resulting in $\Delta\rho \sim \theta_{sH}^2$. Instead, one should focus on the spin polarization s^y, described by the wavenumbers q_{sg} and q_{isg}, which represent the efficiency of the conversion of an electric field to a spin polarization, and vice versa. Therefore, our theory is a generalization of previous approaches [39] which focus on the spin Hall angle and the spin currents.

Last but not least, our results compare favorably with experiments on hybrid structures consisting of spin–orbit active materials and a ferromagnetic metal. In these measurements, the γ scan is usually explained by an additional contribution from the anisotropic magnetoresistance [4, 52, 53]. Note, however, that the measured signals also qualitatively agree with the magnetoresistance obtained in this work for a field-like torque, see figure 3. Since the spin mixing conductance is determined by interface properties, it is not obvious that its imaginary part is always negligible. Therefore, special care is required when interpreting the measured signals. For example, the magnetoresistance in a Bi(15 nm)/Ag/CoFeB trilayer, where a Rashba 2DEG is present at the Bi/Ag interface, shows a sign reversal in the oscillation of the γ scan when comparing the low-temperature with the room-temperature measurements [17]. Qualitatively, the signals in the first case agree with figure 3(a), and in the second case with figure 3(b). Since $1/\tau$ is typically an increasing function of the temperature and $\tau_{DP}/\tau_s \sim 1/\tau^2$, the ratio $\tilde{q}_1/\tilde{q}_2$ is also temperature dependent. Hence, figure 3(a) with $\tilde{q}_1/\tilde{q}_2 < 1$ due to a small ratio $\tau_{DP}/\tau_s = 0.5$ corresponds to the low-temperature regime and, vice versa, figure 3(b) with $\tilde{q}_1/\tilde{q}_2 > 1$ to the high-temperature case.

5. Conclusions

We have presented a microscopic theory of the magnetoresistance in bilayer structures consisting of a Rashba metal and a ferromagnetic insulator, where the Rashba metal exhibits a mass anisotropy. Extrinsic spin–orbit coupling due to impurities has been taken into account via Elliott–Yafet spin relaxation, as well as side-jump and skew scattering. The mass anisotropy of the Rashba metal leads to an anisotropic Elliott–Yafet spin relaxation mechanism. Consequently, and enhanced by Dyakonov–Perel spin relaxation, the spin diffusion equations contain two different spin relaxation lengths. Notably, the angular dependence of the magnetoresistance is fully determined by the current-induced spin polarization. In order to illustrate the relevance of the Rashba-metal/ferromagnet interface, we have considered a purely damping-like and a purely field-like torque, respectively. In both cases, the magnitude of the magnetoresistance is strongly enhanced when Rashba spin–orbit coupling is large compared to extrinsic contributions. Interestingly, for a field-like torque the γ scan acquires a nonzero amplitude whose sign is determined by the ratio of the two spin relaxation lengths, and is thus directly related to the anisotropy of the spin relaxation. Due to the temperature dependence of the spin relaxation lengths, a sign change in the amplitude of the γ scan is predicted, consistent with the experimentally observed temperature dependence. A careful analysis of the experimental data will therefore provide important information concerning the anisotropy of the spin relaxation mechanism and its temperature dependence.

Our conclusions are expected to apply to 3D intrinsic Rashba metals [33–35], to thin metallic bilayers at low temperature [37], and to materials with built-in anisotropy from 'decoration' with nanoislands [38].

Acknowledgments

Appendix A. Kinetic theory

The spin–orbit interaction in equation (2) can be rewritten in terms of spin-dependent vector potentials [44, 54–57]. We adopt this point of view and employ the generalized Boltzmann equation derived in [44]. In the static case it reads

$$\frac{\mathrm{i}}{\hbar}\frac{\mathbf{p}}{m_{\parallel}}\cdot\left[\mathcal{A}^a\frac{\sigma^a}{2},f\right]+\frac{p_z}{m_{\perp}}f+\frac{1}{2}\{\boldsymbol{\mathcal{F}}\cdot\nabla_{\mathbf{p}},f\}=I_0+I_{\mathrm{EY}}+I_{\mathrm{ext}}.\tag{A1}$$

Here, we have assumed that the system is homogeneous in the xy plane and inhomogeneous for $z>0$ due to the attachment to the ferromagnet at $z=0$. The nonzero components of the SU(2) vector potential and the SU(2) Lorentz force with the electric field $E_x\mathbf{e}_x$ are given by

$$\mathcal{A}^x_y=-\mathcal{A}^y_x=\frac{\hbar}{l_{\mathrm{DP}}},\tag{A2}$$

$$\boldsymbol{\mathcal{F}}=-eE_x\mathbf{e}_x-\frac{\mathbf{p}}{m_{\parallel}}\times\boldsymbol{\mathcal{B}}^a\frac{\sigma^a}{2},\tag{A3}$$

where the only nonzero component of the SU(2) magnetic field $\mathcal{B}^a_i$ is $\mathcal{B}^z_z=-\hbar/l^2_{\mathrm{DP}}$. The collision operators on the rhs of the Boltzmann equation (A1) describe momentum relaxation (I_0) with the relaxation rate $1/\tau$, Elliott–Yafet spin relaxation (I_{EY}) associated with the relaxation rate $1/\tau_s$, and side-jump and skew scattering (I_{ext}, see [28] for details). More precisely, the Elliott–Yafet collision operator consists of

$$I^0_{\mathrm{EY}}=-\frac{1}{\tau_s}\boldsymbol{\sigma}\cdot(\Gamma\langle\mathbf{f}\rangle),\tag{A4}$$

where $\langle...\rangle$ denotes the angular average and $\Gamma=\mathrm{diag}(1,1,\zeta)$ accounts for the anisotropy of Elliott–Yafet spin relaxation. In addition, the Elliott–Yafet collision operator yields the following linear in the SU(2) potential contributions:

$$I^{\mathcal{A}}_{\mathrm{EY},s}=\frac{1}{N_0\tau}\left(\frac{\lambda}{2\hbar}\right)^4\mathcal{A}^a_i\varepsilon_{ijk}\varepsilon_{lmn}\int\frac{\mathrm{d}^3p'}{(2\pi\hbar)^3}\delta(\epsilon_{\mathbf{p}}-\epsilon_{\mathbf{p}'})(f^0_{\mathbf{p}'}-f^0_{\mathbf{p}})$$
$$\times[p'_kp'_np_m\delta_{jl}\sigma^a-p'_np_kp_m(\delta_{aj}\sigma^l+\delta_{al}\sigma^j-\delta_{jl}\sigma^a)],\tag{A5}$$

$$I_{\mathrm{EY},c}^{\mathcal{A}} = \frac{1}{N_0\tau}\left(\frac{\lambda}{2\hbar}\right)^4 \mathcal{A}_i^a \varepsilon_{ijk}\varepsilon_{lmn}\int \frac{\mathrm{d}^3 p'}{(2\pi\hbar)^3}\delta(\epsilon_{\mathbf{p}} - \epsilon_{\mathbf{p}'})p'_k\, p'_n\, p_m$$
$$\times\, [f_{\mathbf{p}'}^b(\delta_{al}\delta_{bj} + \delta_{aj}\delta_{bl}) - \delta_{ab}\delta_{jl}(f_{\mathbf{p}'}^b + f_{\mathbf{p}}^b)], \tag{A6}$$

where $\epsilon_{\mathbf{p}} = (p_x^2 + p_y^2)\big/2m_{\parallel} + p_z^2\big/m_{\perp}$ is the band energy and $s\,(c)$ denotes a contribution to the spin (charge) sector. The above collision operators, equations (A4)–(A6), are obtained by following the outline given in [44] with the self-energies

$$\tilde{\Sigma}_{\mathrm{EY}}^0 = \frac{1}{2\pi\hbar N_0\tau}\left(\frac{\lambda}{2\hbar}\right)^4\int\frac{\mathrm{d}^3 p'}{(2\pi\hbar)^3}[(\mathbf{p}\times\mathbf{p}')\cdot\boldsymbol{\sigma}]\tilde{G}(\mathbf{p}')[(\mathbf{p}\times\mathbf{p}')\cdot\boldsymbol{\sigma}], \tag{A7}$$

$$\tilde{\Sigma}_{\mathrm{EY}}^{\mathcal{A}} = \frac{1}{4\pi\hbar N_0\tau}\left(\frac{\lambda}{2\hbar}\right)^4\left\{\mathcal{A}_i^a\sigma^a,\nabla_{p_i}\int\frac{\mathrm{d}^3 p'}{(2\pi\hbar)^3}[(\mathbf{p}\times\mathbf{p}')\cdot\boldsymbol{\sigma}]\tilde{G}(\mathbf{p}')[(\mathbf{p}\times\mathbf{p}')\cdot\boldsymbol{\sigma}]\right\}$$
$$-\frac{1}{4\pi\hbar N_0\tau}\left(\frac{\lambda}{2\hbar}\right)^4\int\frac{\mathrm{d}^3 p'}{(2\pi\hbar)^3}[(\mathbf{p}\times\mathbf{p}')\cdot\boldsymbol{\sigma}]\{\mathcal{A}_i^a\sigma^a,(\nabla_{p_i'}\tilde{G}(\mathbf{p}'))\}[(\mathbf{p}\times\mathbf{p}')\cdot\boldsymbol{\sigma}], \tag{A8}$$

where $\{\cdot,\cdot\}$ denotes the anti-commutator and $\tilde{G}$ is the locally covariant Green's function in Keldysh space. Although not explicitly indicated, the self-energies and Green's function are taken as impurity averaged. For more details on the Elliott–Yafet collision operator we refer, for instance, to [30, 58].

By performing the trace of the Boltzmann equation (A1), multiplying with p_x, performing the momentum integration, and rearranging the terms one obtains the charge current j_x as given in equation (28). In order to derive the spin diffusion equations (11)–(13) we consider the trace of the Boltzmann equation after multiplication with the Pauli vector, $\mathrm{Tr}[\boldsymbol{\sigma}/2\,...]$. From the resulting 3×3 matrix equation we can obtain two equations for the spin density and the spin current: first, a direct integration over the momentum yields

$$\Gamma\mathbf{s} + \tau_s\nabla_z\mathbf{j}_z - \tau_s\frac{\mathcal{A}_i}{\hbar}\times\mathbf{j}_i = \mathbf{e}_y\theta_{\mathrm{int}}^{\mathrm{sH}}\frac{\tau_{\mathrm{DP}}}{l_{\mathrm{DP}}}\left(1 - \frac{3\zeta}{4}\right)\frac{\sigma_{\mathrm{D}}E_x}{2e}. \tag{A9}$$

Second, solving for $\mathbf{f}$ in terms of $\langle\mathbf{f}\rangle$ and f^0, and performing the momentum integration after a multiplication by p_i with $i = x, y, z$ yields the spin currents

$$\mathbf{j}_x = -\frac{l_{\mathrm{DP}}}{\tau_{\mathrm{DP}}}\mathbf{e}_y\times\mathbf{s}, \tag{A10}$$

$$\mathbf{j}_y = \frac{l_{\mathrm{DP}}}{\tau_{\mathrm{DP}}}\mathbf{e}_x\times\mathbf{s} + \mathbf{e}_z(\theta_{\mathrm{int}}^{\mathrm{sH}} + \theta_{\mathrm{ext}}^{\mathrm{sH}})\frac{\sigma_{\mathrm{D}}E_x}{2e}, \tag{A11}$$

$$\mathbf{j}_z = -D_{\perp}\nabla_z\mathbf{s} - \mathbf{e}_y\theta_{\mathrm{ext}}^{\mathrm{sH}}\frac{m_{\parallel}}{m_{\perp}}\frac{\sigma_{\mathrm{D}}E_x}{2e}. \tag{A12}$$

The spin diffusion equations (11)–(13) now follow from inserting equations (A10)–(A12) into equation (A9).

Appendix B. Spin diffusion equations

In this appendix we briefly outline how to solve the spin diffusion equations (11)–(13) for the current-induced spin polarization s^y as described by equations (19)–(25). Since we deal with decoupled differential equations, the general solution is easily obtained,

$$s^x = a_1 e^{-q_1 z} + a_2 e^{q_1 z}, \tag{B1}$$

$$s^y = b_1 e^{-q_1 z} + b_2 e^{q_1 z} + s_0^y, \tag{B2}$$

$$s^z = c_1 e^{-q_2 z} + c_2 e^{q_2 z}, \tag{B3}$$

respectively. The boundary conditions as given in the main text, $\mathbf{j}_z(d) = 0$ and equation (1), can be applied to equations (B1)–(B3) by employing equation (A12). Considering first $\mathbf{j}_z(d) = 0$, we can reduce the number of unknown parameters,

$$s^x = a\cosh(q_1(d - z)), \tag{B4}$$

$$s^y = b\cosh(q_1(d - z)) + \frac{\theta_{\mathrm{ext}}^{\mathrm{sH}}\sigma_{\mathrm{D}}E_x}{2eq_1 D_{\parallel}}\sinh(q_1(d - z)) + s_0^y, \tag{B5}$$

$$s^z = c\cosh(q_2(d - z)). \tag{B6}$$

It is now convenient to begin with the case without ferromagnet, i.e., $\mathbf{j}_z(0) = 0$. In this case, the spin density s^y is given by

$$s^y(z)|_{q_r=q_i=0} = s_0^y + \Delta s_{sc}^y(z), \tag{B7}$$

with Δs_{sc}^y as given in equation (20). In the presence of the ferromagnet, the spin density can be written as follows:

$$\mathbf{s}(z, \mathbf{n}) = [s_0^y + \Delta s_{sc}^y(z)]\mathbf{e}_y + \Delta\mathbf{s}(z, \mathbf{n}), \tag{B8}$$

where

$$\Delta\mathbf{s}(z, \mathbf{n}) = \begin{pmatrix} \tilde{a}\cosh(q_1(d-z)) \\ \tilde{b}\cosh(q_1(d-z)) \\ \tilde{c}\cosh(q_2(d-z)) \end{pmatrix}. \tag{B9}$$

By splitting the spin current $\mathbf{j}_z$ similar to equation (B8), the application of the boundary condition (1) leads to

$$\begin{pmatrix} q_1\tilde{a}\sinh(q_1 d) \\ q_1\tilde{b}\sinh(q_1 d) \\ q_1\tilde{c}\sinh(q_2 d) \end{pmatrix} = D_\perp q_r\mathbf{n}\times[\mathbf{n}\times\mathbf{s}(0)] + D_\perp q_i\mathbf{n}\times\mathbf{s}(0) \tag{B10}$$

with

$$\mathbf{s}(0) = [s_0^y + \Delta s_{sc}^y(0)]\mathbf{e}_y + \begin{pmatrix} \tilde{a}\cosh(q_1 d) \\ \tilde{b}\cosh(q_1 d) \\ \tilde{c}\cosh(q_2 d) \end{pmatrix}. \tag{B11}$$

The remaining task is now to solve for $\tilde{b}$. One way is to parameterize $\mathbf{n}$ in spherical coordinates and multiply equation (B10) by the rotation matrix $\mathbb{D}$ with the property $\mathbb{D}\mathbf{n} = \mathbf{e}_x$. By a proper choice of the spherical angles regarding the α, β, and γ scans, respectively, the solution for $\tilde{b}$ of the resulting system of linear equations finally yields the spin density $\Delta s_{\alpha,\beta,\gamma}^y$ as given by equations (21)–(25).

ORCID iDs

Sebastian Tölle ⓘ https://orcid.org/0000-0002-4189-7083
Ulrich Eckern ⓘ https://orcid.org/0000-0001-8917-9083

References

[1] Žutić I, Fabian J and Sarma S D 2004 *Rev. Mod. Phys.* **76** 323
[2] Sinova J, Valenzuela S O, Wunderlich J, Back C H and Jungwirth T 2015 *Rev. Mod. Phys.* **87** 1213
[3] Nakayama H *et al* 2013 *Phys. Rev. Lett.* **110** 206601
[4] Avci C O, Garello K, Ghosh A, Gabureac M, Alvarado S F and Gambardella P 2015 *Nat. Phys.* **11** 570
[5] Han J H, Song C, Li F, Wang Y Y, Wang G Y, Yang Q H and Pan F 2014 *Phys. Rev.* B **90** 144431
[6] Dyakonov M and Perel V 1971 *Phys. Lett.* A **35** 459
[7] Hirsch J E 1999 *Phys. Rev. Lett.* **83** 1834
[8] Kato Y K, Myers R C, Gossard A C and Awschalom D D 2004 *Science* **306** 1910
[9] Wunderlich J, Kaestner B, Sinova J and Jungwirth T 2005 *Phys. Rev. Lett.* **94** 047204
[10] Slonczewski J 1996 *J. Magn. Magn. Mater.* **159** L1
[11] Berger L 1996 *Phys. Rev.* B **54** 9353
[12] Tsoi M, Jansen A G M, Bass J, Chiang W-C, Seck M, Tsoi V and Wyder P 1998 *Phys. Rev. Lett.* **80** 4281
[13] Zhao H, Loren E J, van Driel H M and Smirl A L 2006 *Phys. Rev. Lett.* **96** 246601
[14] Saitoh E, Ueda M, Miyajima H and Tatara G 2006 *Appl. Phys. Lett.* **88** 182509
[15] Valenzuela S O and Tinkham M 2006 *Nature* **442** 176
[16] Nakayama H, Kanno Y, An H, Tashiro T, Haku S, Nomura A and Ando K 2016 *Phys. Rev. Lett.* **117** 116602
[17] Nakayama H, An H, Nomura A, Kanno Y, Haku S, Kuwahara Y, Sakimura H and Ando K 2017 *Appl. Phys. Lett.* **110** 222406
[18] Ivchenko E L and Pikus G E 1978 *JETP Lett.* **27** 604
[19] Vas'ko F T and Prima N A 1979 *Sov. Phys. Solid State* **21** 994
[20] Aronov A G and Lyanda-Geller Y B 1989 *JETP Lett.* **50** 431
[21] Kato Y K, Myers R C, Gossard A C and Awschalom D D 2004 *Phys. Rev. Lett.* **93** 176601
[22] Silov A Y, Blajnov P A, Wolter J H, Hey R, Ploog K H and Averkiev N S 2004 *Appl. Phys. Lett.* **85** 5929
[23] Edelstein V 1990 *Solid State Commun.* **73** 233
[24] Rashba É I 1960 *Sov. Phys. Solid State* **2** 1109
[25] Bychkov Y A and Rashba É I 1984 *JETP Lett.* **39** 78
[26] Ganichev S D, Ivchenko E L, Danilov S N, Eroms J, Wegscheider W, Weiss D and Prettl W 2001 *Phys. Rev. Lett.* **86** 4358
[27] Ganichev S D, Ivchenko E L, Bel'kov V V, Tarasenko S A, Sollinger M, Weiss D, Wegscheider W and Prettl W 2002 *Nature* **417** 153
[28] Raimondi R, Schwab P, Gorini C and Vignale G 2012 *Ann. Phys., Berlin* **524** 153
[29] Grigoryan V L, Guo W, Bauer G E W and Xiao J 2014 *Phys. Rev.* B **90** 161412
[30] Tölle S, Eckern U and Gorini C 2017 *Phys. Rev.* B **95** 115404
[31] Tölle S, Dzierzawa M, Eckern U and Gorini C 2018 *Ann. Phys., Berlin* **530** 1700303
[32] Dugaev V K, Inglot M, Sherman E Y, Berakdar J and Barnaś J 2012 *Phys. Rev. Lett.* **109** 206601

[33] Ishizaka K *et al* 2011 *Nat. Mater.* **10** 521

[34] Niesner D, Wilhelm M, Levchuk I, Osvet A, Shrestha S, Batentschuk M, Brabec C and Fauster T 2016 *Phys. Rev. Lett.* **117** 126401

[35] Martin C, Suslov A V, Buvaev S, Hebard A F, Bugnon P, Berger H, Magrez A and Tanner D B 2017 *Europhys. Lett.* **116** 57003

[36] Brosco V and Grimaldi C 2017 *Phys. Rev.* B **95** 195164

[37] Ryu J, Kohda M and Nitta J 2016 *Phys. Rev. Lett.* **116** 256802

[38] Zhou L *et al* 2018 *Sci. Adv.* **4** eaao3318

[39] Chen Y-T, Takahashi S, Nakayama H, Althammer M, Goennenwein S T B, Saitoh E and Bauer G E W 2013 *Phys. Rev.* B **87** 144411

[40] Kovalev A A, Brataas A and Bauer G E W 2002 *Phys. Rev.* B **66** 224424

[41] Slonczewski J C 2002 *J. Magn. Magn. Mater.* **247** 324

[42] Chen K and Zhang S 2015 *Phys. Rev. Lett.* **114** 126602

[43] Vélez S, Golovach V N, Gomez-Perez J M, Bui C T, Rivadulla F, Hueso L E, Bergeret F S and Casanova F 2018 arXiv:1805.11225

[44] Gorini C, Schwab P, Raimondi R and Shelankov A L 2010 *Phys. Rev.* B **82** 195316

[45] Mishchenko E G, Shytov A V and Halperin B I 2004 *Phys. Rev. Lett.* **93** 226602

[46] Shytov A V, Mishchenko E G, Engel H-A and Halperin B I 2006 *Phys. Rev.* B **73** 075316

[47] Raimondi R, Gorini C, Schwab P and Dzierzawa M 2006 *Phys. Rev.* B **74** 035340

[48] Khaetskii A 2006 *Phys. Rev.* B **73** 115323

[49] Adagideli I and Bauer G E W 2005 *Phys. Rev. Lett.* **95** 256602

[50] Schwab P, Dzierzawa M, Gorini C and Raimondi R 2007 *Phys. Rev.* B **74** 155316

[51] Adagideli I, Scheid M, Wimmer M, Bauer G E W and Richter K 2007 *New J. Phys.* **9** 382

[52] Liu J, Ohkubo T, Mitani S, Hono K and Hayashi M 2015 *Appl. Phys. Lett.* **107** 232408

[53] Kim J, Sheng P, Takahashi S, Mitani S and Hayashi M 2016 *Phys. Rev. Lett.* **116** 097201

[54] Mathur H and Stone A D 1992 *Phys. Rev. Lett.* **68** 2964

[55] Lyanda-Geller Y 1998 *Phys. Rev. Lett.* **80** 4273

[56] Tokatly I V 2008 *Phys. Rev. Lett.* **101** 106601

[57] Tokatly I V and Sherman E Y 2010 *Ann. Phys., NY* **325** 1104

[58] Gorini C, Maleki Sheikhabadi A, Shen K, Tokatly I V, Vignale G and Raimondi R 2017 *Phys. Rev.* B **95** 205424